Peer-reviewed version available at *Nanomaterials* **2018**, *8*, 446; doi:10.3390/nano8060446

Article

MIL-100(Al) gels as an excellent platform loaded with doxorubicin hydrochloride for pH-triggered drug release and anticancer effect

Yuge Feng [1], Chengliang Wang [2], Fei Ke [3], Jianye Zang [2] and Junfa Zhu [1,*]

[1] National Synchrotron Radiation Laboratory and Department of Chemical Physics, University of Science and Technology of China, China; ygfeng@mail.ustc.edu.cn

[2] Hefei National Laboratory for Physical Sciences at Microscale, CAS Center for Excellence in Biomacromolecules, Collaborative Innovation Center of Chemistry for Life Sciences, and School of Life Sciences, University of Science and Technology of China, China; wangcl@ustc.edu.cn; zangjy@ustc.edu.cn

[3] Department of Applied Chemistry and State Key Laboratory of Tea Plant Biology and Utilization, Anhui Agricultural University, China; kefei@ahau.edu.cn

* Correspondence: jfzhu@ustc.edu.cn; Tel.: +86-551-63602064

Abstract: Slow and controlled release systems for drugs, have attracted increasing interest recently. A highly efficient metal-organic gels (MOGs) drug delivery carrier, i.e., MIL-100(Al) gels, has been fabricated by a facile, low cost and environment friendly one-pot process. The unique structure of MIL-100(Al) gels leads to a high loading efficiency (620 mg/g) towards doxorubicin hydrochloride (DOX) as a kind of anticancer drugs. DOX-loaded MOGs exhibited high stability under physiological conditions and sustained release capacity of DOX for up to 3 days (under acidic environments). They further showed sustained drug release behavior and excellent antitumor effects in in vitro experiments on HeLa cells, in contrast with the extremely low biotoxicity of MOGs. Our work provides a promising way for the anticancer therapy, by utilizing this MOGs-based drug delivery system, as an efficient and safe vehicle.

Keywords: Metal-organic gels; Doxorubicin loading and release; pH-responsiveness; anticancer effect

1. Introduction

Most Anticancer chemotherapeutics were controlled at high doses to make up for their premature deterioration and non-specific absorption, which typically results in the development of dose-limited toxicity [1-4]. As alternatives, slow and controlled release systems for drugs, have attracted increasing interest recently [5,6]. On the one hand, continuous slow and sustained release of small amounts of drug, instead of several large doses, can weaken patient compliance [7]. On the other hand, delivering the drug by controlled release can reduce the side effects thus improve therapeutic efficiency [8].

Metal-organic framework (MOF) is a class of crystalline porous hybrids built from metal ions and organic linkers. Its large surface area, tunable pore size, adjustable composition and structure, and versatile functionality character, make it an ideal carrier for slow and controlled release drug delivery [9-15]. For instance, Horcajada et al. reported that MIL-100(Fe) nanoparticles could load anticancer drug (doxorubicin, DOX) up to 9%, and a sustained release in PBS within 14 days was observed [16]. Sun et al. reported Cu-metal organic frameworks (MOFs), MOFs-2 and MOFs-3, and their application as the transport vehicles for the delivery of doxorubicin hydrochloride (DOX). The MOFs-2 showed the best performance in transport DOX as the consequence of highest loading capacity (95 mg/g). In weak acid solution (pH 5.8), MOFs-2 released 20% DOX in 80 h [17]. Vasconcelos et al. encapsulated anticancer drug DOX in nano ZIF-8 with a loading capacity of 49 mg/g, which exhibited a progressive release behavior [18]. However, every previous study has its own shortcoming, including complicated synthesis routes, intrinsic biotoxicity, low loading capacity, short release time and poor stability at a physiological pH of 7.4. The shortcomings limit their potential applications in clinical treatment, which requires high qualities of all the performance-indicators as mentioned above.

Metal-organic gels (MOGs), as the emerging carriers, are constructed by the self-assembly of metal ions and suitable ligands through various noncovalent interactions [19,20]. Compared with MOFs, MOGs possess lower density, higher surface area, larger porosity and can be synthesized in gentle conditions, such as cheap and clean solution, low temperature and short reaction time [21-27]. Inspired by these outstanding features, herein, we have designed a kind of MOGs, i.e., MIL-100(Al) gels synthesized by a facile, low cost and environment friendly one-pot process, as the carrier for anticancer drug doxorubicin (DOX). It is encouraging that MIL-100(Al) gels exhibit high performance in all the typical indicators. Firstly, they involve concise synthetic step, large loading capacity for DOX and low biotoxicity. Secondly, DOX-loaded MOGs show slow and sustainable releasing ability and high anticancer efficiency, thus providing promising approach for the clinical anticancer treatment.

2. Materials and Methods

2.1. Materials and methods

1,3,5-Benzenetricarboxylic acid (H_3BTC) was purchased from Sigma-Aldrich (St. Louis, MO, USA). Aluminium nitrate nonahydrate ($Al(NO_3)_3 \bullet 9H_2O$) was obtained from Sinopharm (Shanghai) Chemical Reagent Co., Ltd., China. Doxorubicin (DOX) was purchased from Aladdin Biotech Company (Shanghai, China). Other chemicals obtained from commercial suppliers were of analytical reagent. All chemicals were used without further purification.

The powder X-ray diffraction (PXRD) patterns was collected by using the Theta Rotating anode X-ray Diffractometer with Cu target (40 KV, 200mA) from 2° to 70°. FTIR spectrum was determined using a Magna-IR 750 spectrometer in the range of 500–4000 cm−1 with a resolution of 4 cm−1. The morphologies of the sample were studied using a SIRION200 Schottky field emission scanning electron microscope and JEM-2100F transmission electron microscope at 200 kV, respectively. Nitrogen adsorption-desorption isotherms were carried out with a Micromeritics TriStar II 3020 adsorption analyzer at 77 K. UV-vis absorption spectra were carried out with a Shimadzu UV-1800 spectrophotometer.

2.2. Synthesis of MIL-100(Al) gels

In a typical synthesis procedure, aluminium nitrate nonahydrate ($Al(NO_3)_3 \bullet 9H_2O$, 7.6 mmol) and 1,3,5-benzentricarboxylic acid (H_3BTC, 5 mmol) were added to 36 mL ethanol [28]. After stirring for 15 min at room temperature to dissolve the solid, the transparent mixture was transferred to a sealed container and heated to 120 ℃ for one hour. The wet gels were dried in an oven at 80 ℃. The finally obtained particles were washed by Soxhlet extractor using ethanol as medium.

2.3. Incorporation of DOX

DOX-anticancer drug (10 mg) was firstly dissolved in 4 mL deionized water and then the MIL-100(Al) gels (10 mg) were added. The suspension was stirred for 24 h in dark at room temperature. The obtained materials were then centrifuged, washed with deionized water for several times and dried under vacuum condition for further release tests. The supernatant was collected and measured by UV-vis spectrophotometer at a wavelength of 480 nm for the calculation of drug loading content and drug loading efficiency. The drug loading capacity was calculated as follows: drug loading capacity = (weight of DOX in MIL-100(Al) gels /weight of nanoparticles). The drug loading efficiency was calculated by: Drug loading efficiency (wt %) = (weight of DOX in MIL-100(Al) gels /weight of feeding DOX) × 100.

Peer-reviewed version available at Nanomaterials 2018, 8, 446; doi:10.3390/nano8060446

2.4. Drug release

The drug release experiment was performed by soaking the sample in PBS buffer solutions (pH = 7.4 and pH = 5.5) at 37 ℃. 10 mg of DOX-loaded MIL-100(Al) gels (DOX-loaded MOGs) were suspended into 10 mL PBS solution. The mixture solution was stirred at the temperature of 37 ℃ in a water bath. At predetermined time intervals, 3 mL of PBS solution was removed and assayed. The volume of each withdrawn sample was replaced by the same volume of fresh PBS solution. The amount of released DOX was calculated according to the absorption analyzed by UV-vis spectrophotometer at 480 nm and standard absorbance vis DOX concentration curve. The calibration experiment was performed using different known concentrations of DOX in PBS buffer solution (shown in Figure S1). The derived standard absorbance vis DOX concentration curve is shown in Figure S2.

2.5. Cell cytotoxicity of DOX-loaded MOGs

HeLa cell was used for cell viability assay. A 96 well plate was used for cell seeding with total number about 2×10^3 per well. The cells were first incubated overnight, and then the MIL-100(Al) gels and DOX-loaded MOGs were added in every well with a final concentration ranging from 0.1 μg/mL to 100μg/mL (0.1 μg/mL, 0.5 μg/mL, 1 μg/mL, 2.5 μg/mL, 5 μg/mL, 10 μg/mL, 25 μg/mL, 50 μg/mL, and 100 μg/mL). Autoclave water was added and treated as negative control. The cells were incubated with MOGs or DOX-loaded MOGs for 12, 24, 36, 48, 72 hours, respectively. Later, all the medium in the wells were drawn and discharged, additional MTT solution dissolved in the medium was used to treat the cells for another 4 hours. Finally, DMSO was loaded to replace the medium and dissolve the crystals for further absorbance detection. The absorbance of each well was obtained at the wavelength of 590 nm. Compared to the negative control, the cell viability were calculated. Each sample were repeated for 5 times and the results were presented as average values with error bars representing standard deviation.

2.6. Flow cytometry

HeLa cells (2×10^5) were seeded on six-well plate and incubated overnight. In the next day, cells were incubated with MIL-100(Al) gels (12.5 μg/mL), DOX-loaded MOGs (12.5 μg/mL) and autoclave water overnight, respectively. The cells were washed twice with 1X PBS followed by treated with 1X trypsin for 5 min before quenching the cells with culture medium. Thereafter, the cells were washed twice with 1X PBS by centrifugation (1000 rpm, 5 min), and 1X ANNEXIN binding buffer (100 μL) was added to the cell together with PI-PE and ANNEXIN V-FITC conjugate. The cells were incubated in the dark for 20 min. Then, they were immediately analyzed with flow cytometer.

2.7. Fluorescence microscopy images

The fluorescence microscopy studies were performed on HeLa cells in a confocal dish with total number of 4×10^5 per dish. MIL-100(Al) gels (200 μL) and DOX-loaded MOGs (200 μL) were added into each dish respectively, to give a final concentration of 12.5 μg/mL and incubated cells for 12 h. Thereafter, the medium was removed and the cells were washed 3 times with 1X PBS. The treated cells were re-suspended in 1X PBS. Then added ANNEXIN V – FITC conjugate (25 μL), and incubated the cells for 15 min in the dark. Thereafter, the ANNEXIN containing PBS was removed and the cells were washed 3 times with 1X PBS before fixing them with paraformaldehyde solution (4% in 1X PBS, 1 mL). After 20 min, removed the formaldehyde solution and washed the cells twice with 1X PBS. In the end, the cells were incubated with Hoechst solution (5 μg/ mL, 1 mL) in 1X PBS in the dark for 15 min, and washed with twice with 1X PBS to image.

Peer-reviewed version available at Nanomaterials 2018, 8, 446; doi:10.3390/nano8060446

3. Results and Discussion

3.1. Morphology and structure characterization of MIL-100(Al) gels

Transmission electron microscope (TEM) images (Fig. 1 a, b) show the irregular structure of the as-synthesized MIL-100(Al) gels. Powder X-ray diffraction (XRD) was applied to identify their microstructure. As depicted in Fig. S1, the XRD result reveals a close relationship to the simulated patterns of single-crystal MIL-100(Al). It shows that the corresponding peaks observed for the MIL-100(Al) crystal also appear in the obtained gel, suggesting that the gel maintains a similar porous structure as that of the MIL-100(Al) crystal. The nitrogen adsorption-desorption isotherm, which was used to evaluate the porous properties of MIL-100(Al) gels, is between those of type-I and type-IV, suggesting the coexistence of micropores and mesopores in the MIL-100(Al) gels sample (Fig. S2). The Brunauer–Emmett–Teller (BET) surface area and pore volume of the MIL-100(Al) gels were calculated to be 920 m^2/g and 0.535 cm^3/g, respectively. Thus, the large surface area and high porosity make this material to be possible used for highly efficient drug loading.

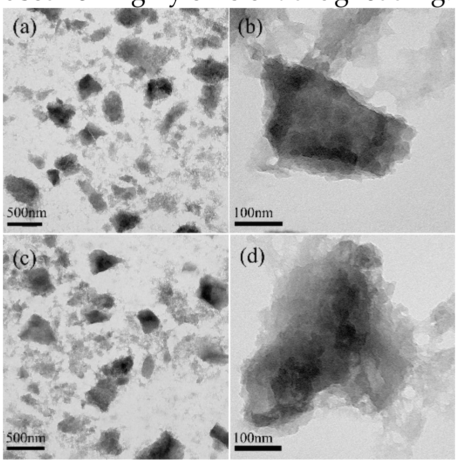

Figure 1. TEM images of (a, b) MIL-100(Al) gels. (c, d) DOX-loaded MIL-100(Al) gels.

3.2. Drug loading and release behaviors

TEM images of DOX-loaded MOGs (Fig. 1c, d) exhibit almost no change in morphology compared with MIL-100(Al) gels. Fig. 2a are XRD patterns of MIL-100(Al) gels and DOX-loaded MIL-100(Al) gels (DOX-loaded MOGs). Both of them show similar features before and after the drug adsorption, indicating that the porous structure of MIL-100(Al) gels is retained after the loading of DOX. Fig. 2b exhibits the FTIR spectra of MIL-100(Al) gels, DOX and DOX-loaded MOGs. The peak at 3400 cm^{-1} is attributed to the O–H stretching of MIL-100(Al) gels. In FTIR spectrum of DOX, peaks at 1020 cm^{-1} and 3400 cm^{-1} are caused by –NH_2 torsional vibration and O–H stretching vibrations of DOX, respectively. In case of DOX-loaded MOGs, peaks of O–H stretching vibrations overlap are broadened and a new adsorption band at 1020 cm^{-1} owing to the torsional vibration of –NH_2 from DOX generate. This FTIR result indicates that MIL-100(Al) gels conjugate with DOX molecules successfully.

Preprints (www.preprints.org) | NOT PEER-REVIEWED | Posted: 30 May 2018 doi:10.20944/preprints201805.0431.v1

Peer-reviewed version available at Nanomaterials 2018, 8, 446; doi:10.3390/nano8060446

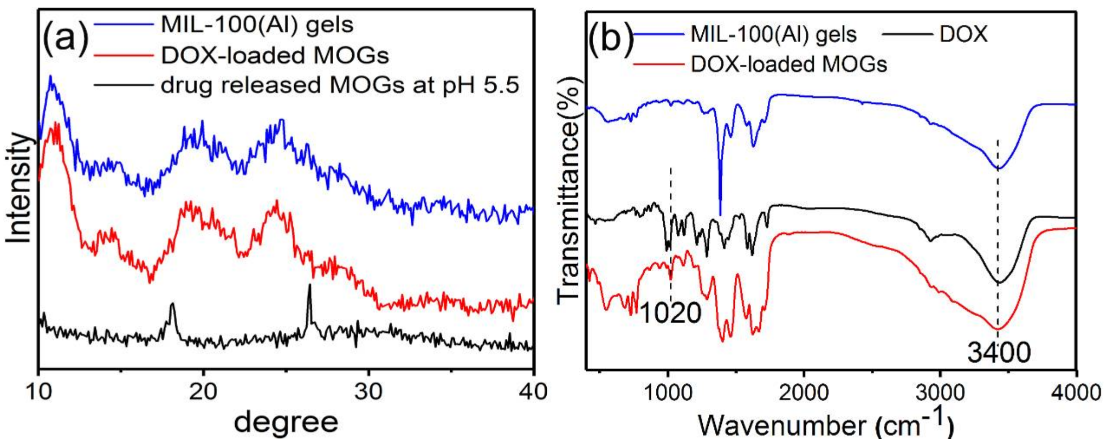

Figure 2. (a) Powder XRD patterns of MIL-100(Al) gels, DOX-loaded MOGs, and drug-released MOGs at pH 5.5; **(b)** FTIR spectra of MIL-100(Al) gels, DOX, and DOX-loaded MOGs.

It turns out that the loading capacity is reached up to 620 mg of DOX per gram of the sample. This large DOX loading capacity and high loading efficiency (62%) may be attributed to the ultrahigh porosity and enormous internal surface of MIL-100(Al) gels. In addition, the interaction between the ammonium groups of DOX and the carboxylate groups of MOGs should be considered as another important reason [29].

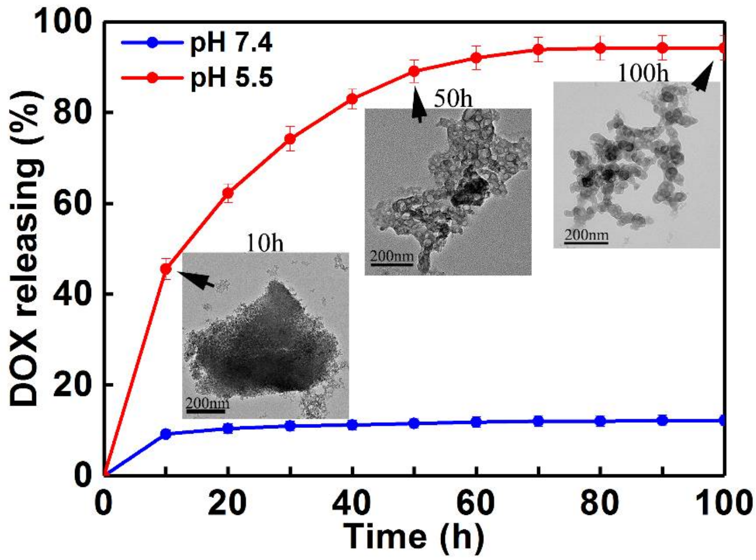

Figure 3. Drug release profiles for DOX-loaded MOGs in PBS buffer solution at pH = 5.5 and pH = 7.4 within 100h. (Inset are TEM images of DOX-loaded MOGs after 10h, 50h and 100h in release process at pH 5.5.) Bars denote the standard deviation (±SD, n = 5).

Controlled drug release kinetics of DOX from DOX-loaded MOGs were investigated using UV-vis adsorption spectra in phosphate-buffered saline (PBS) buffer solutions at 37 ℃. Fig. 3 are the DOX release profiles at two different pH values (pH = 7.4 and 5.5). It can be seen that the release of DOX from DOX-loaded MOGs in pH = 7.4 only reached 10% within 100 h. In contrast, the DOX release rate is significantly increased in pH = 5.5 and this release reached nearly 100% within 100 h. This reveals that under the acidic conditions, the drug can be released more easily. Under the weak acidic condition (pH=5.5), the drug delivery rate gradually decreases with the time. Basically, the rate can be clearly divided into three regions: (i) an early rapid release within the first 10 hours; (ii) a slow release region in the time range between 10 and 60 hours; (iii) a saturation region after 70 hours [30]. The first rapid release is induced by the simple diffusion and dissolution of DOX molecules adsorbed onto the surface of MOGs. The second region reveals a gentle and steady release over a long time, due to the desorption, diffusion, and dissolution processes of DOX molecules from channels in the gels to the solution. The last saturated drug release process could be attributed to host-guest interactions between DOX molecules and the gels. The results revealed that the obtained MIL-100(Al) gels exhibit a high drug loading and long sustained release time under acidic environment. To further understand the DOX release process from DOX-loaded MOGs, TEM images were taken from DOX-loaded MOGs after 10h, 50h and 100h in release process at pH 5.5 (inset in Fig. 3). They revealed gradual collapse of MIL-100(Al) gels structure during the procedure. The result is consistent with the XRD pattern of drug-released MOGs at pH 5.5(Fig. 2a) which shows the dissolution of MIL-100(Al) gels in the acidic environment.

3.3. Cell Cytotoxicity of DOX-loaded MOGs

After evaluating the drug loading and release ability of MOGs, in vitro cell viabilities of DOX-loaded MOGs and pure MIL-100(Al) gels on HeLa cells were investigated using MTT (3-(4,5-Dimethylthiazol-2-yl)-2,5-diphenyltetrazolium bromide) assay. To study the biotoxicity of pure MIL-100(Al) gels and the therapeutic efficiency of DOX-loaded MOGs, HeLa cells were cultured with the DOX-loaded MOGs and pure MIL-100(Al) gels at concentrations ranging from 0.1 μg/mL to 100 μg/mL (0.1, 0.5, 1, 2.5, 5, 10, 25, 50 and 100 μg/mL) for 24h. The results are exhibited in Fig. 4. As can be seen, after 24 h incubation with HeLa cells, the pure MIL-100(Al) gels show no obvious toxicity towards the HeLa cells even at the concentration of the MIL-100(Al) gels as high as 100 μg/mL. In contrast, the DOX-loaded MOGs shows high cytotoxicity on HeLa cells. As the concentration of DOX-loaded MOGs increases, the cell viability rapidly decreases. When the concentration of DOX-loaded MOGs reaches 25 μg/mL, only ~20% of HeLa cells can survive. Therefore, the DOX can be efficiently released from the DOX-loaded MOGs to kill most of the tumor cells, demonstrating that the as-synthesized MIL-100(Al) gels hold a great promise for application in the field of drug delivery system for cancer treatment.

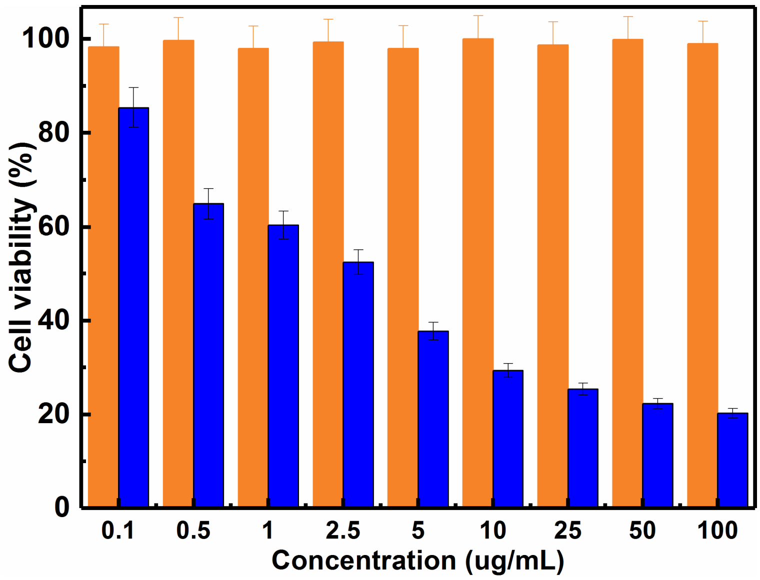

Figure 4. The effect of MIL-100(Al) gels and DOX-loaded MOGs with various concentrations on the cell viability of HeLa cells in 24h (the orange and blue bars represent viability of HeLa cancer cells incubated with MIL-100(Al) gels and DOX-loaded MOGs, respectively).

In vitro drug release behavior of DOX-loaded MOGs on HeLa cells was also investigated. DOX-loaded MOGs and MOGs + free DOX with different concertation were studied. The results are shown in Fig. 5a-f. Accordingly, viability of cells incubated with DOX-loaded MOGs gradually decrease in the time range of 72 h. This is in contrast with the sudden reduction behavior of the viability of cells incubated with MOGs + free DOX, in all the control experiment groups.

Peer-reviewed version available at Nanomaterials 2018, 8, 446; doi:10.3390/nano8060446

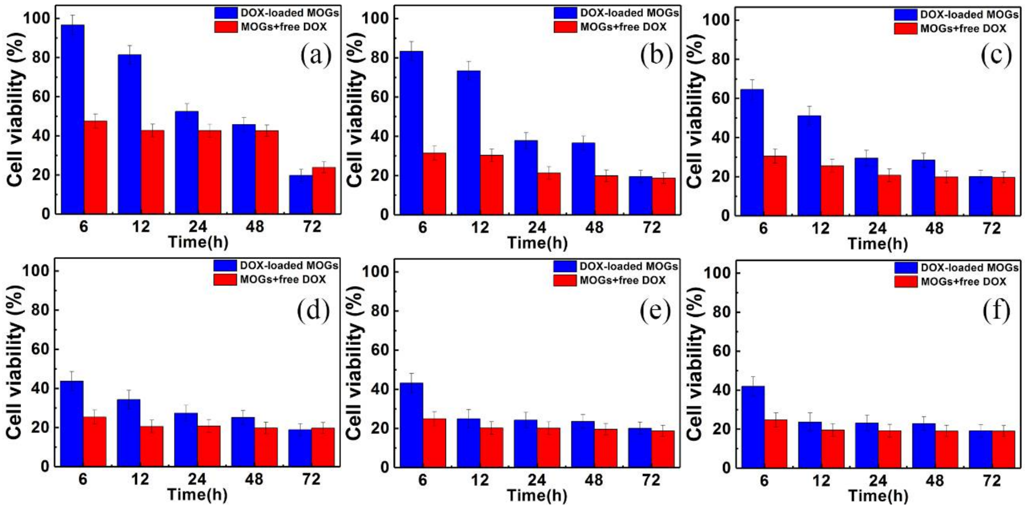

Figure 5. Cell viability of HeLa cells incubated with DOX-loaded MOGs and MOGs + free DOX for different time periods at concentrations of **(a)** 2.5 μg/mL, **(b)** 5 μg/mL, **(c)** 10 μg/mL, **(d)** 25 μg/mL, **(e)** 50 μg/mL, and **(f)** 100 μg/mL.

3.4. Flow cytometry

In order to further investigate the apoptosis of the cells, we performed the flow cytometry analysis on HeLa cells with 12.5 μg/mL MIL-100(Al) gels and DOX-loaded MOGs. As shown in Fig. 6, almost no necrotic and late apoptotic cells were observed at the control experiment (only contains pure autoclave water) (1.49%) MIL-100(Al) gels (1.88%), revealing the low toxicity of this MOGs-based materials. However, when the DOX-loaded MOGs were added, the percentage of apoptotic cells immediately became prominent (89.9%). These results are in line with the MTT assay and further confirm the apoptotic cell death arised from the DOX released from DOX-loaded MOGs.

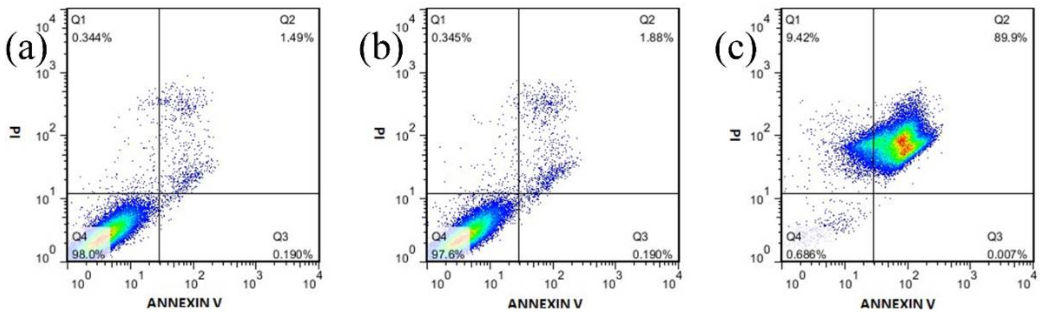

Figure 6. Flow cytommetry experiments of HeLa cells when incubated with **(a)** Pure autoclave water as control, **(b)** MIL-100(Al) gels, and **(c)** DOX-loaded MOGs, respectively.

3.5. Fluorescence microscopy images

To further confirm therapeutic efficiency of DOX-loaded MOGs, we performed the confocal fluorescence microscopy for HeLa cells incubated with 12.5 μg/ml pure MIL-100(Al) gels and DOX-loaded MOGs for 24 h, followed by staining the nucleus with DAPI and the apoptotic cells with Annexin V-FITC. The results are revealed in Fig. 7. Herein, the green fluorescence is attributed to the apoptotic HeLa cells, while the blue and red fluorescence represent the living cell imaging and DOX released, respectively. For the HeLa cells incubated with pure MIL-100(Al) gels, only very small amount of apoptotic HeLa cells is presented (Fig. 7c, d). In contrast, for the HeLa cells incubated with DOX-loaded MOGs, a large number of the HeLa cells are apoptotic (Fig. 7g, h). This result again demonstrates the high efficiency of the DOX-loaded MOGs in the cancer therapeutic treatment.

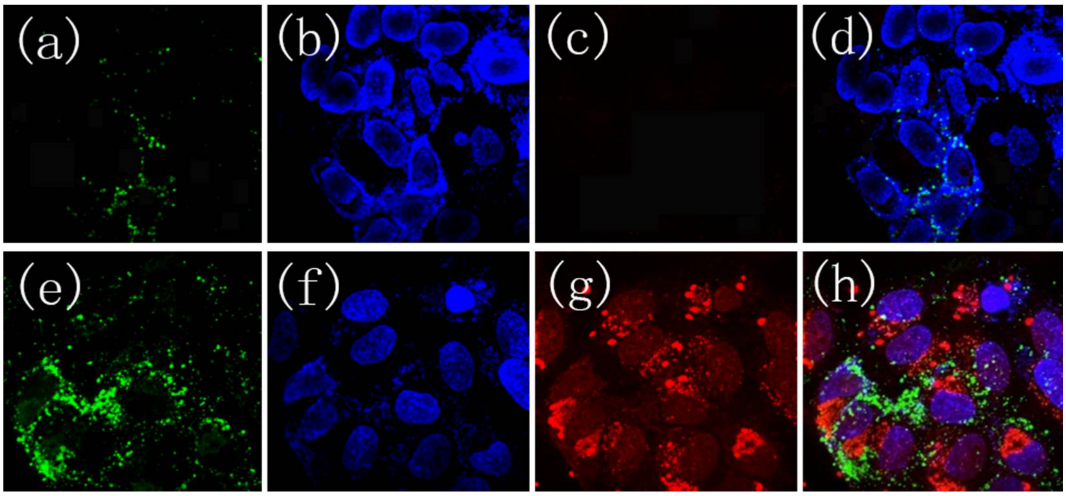

Figure 7. Confocal microscopy images of HeLa cells incubated with 12.5 μg/mL **(a-d)** MIL-100(Al) gels and **(e-h)** DOX-loaded MOGs, respectively. Blue fluorescence represents the living cell imaging. Red fluorescence represents released DOX from DOX-loaded MOGs within the cancer cells. Green fluorescence represents apoptosis of cells. d and h are the merged images of a-c and e-g, respectively.

4. Conclusions

On the basis of the methods reported in the previous work [5,6,19, 20], we report a metal-organic gels (MOGs)-based drug delivery system, for anticancer therapy, i.e., MIL-100(Al) gels, which were synthesized by a facile, low cost and environment friendly one-pot method. The anticancer drug doxorubicin hydrochloride (DOX) can be successfully encapsulated in the MIL-100(Al) gels with high loadings (620 mg/g). Through control experiments, the fabricated DOX-loaded MOGs are comparable with some previous pH-responsive drug delivery system [16-18]. Specifically, the drug was not released at physiological condition (PBS, pH 7.4) but released in a controlled manner at acidic conditions (pH 5.5) with approximately 100%, after delivered over 3 days. We also conducted in vitro experiment of DOX-loaded MIL-100(Al) gels (DOX-loaded MOGs) toward HeLa cells. It turns out that the DOX-loaded MOGs have excellent efficiency in killing the HeLa cells. The synthetic MIL-100(Al) gels here feature concise synthetic step, large loading capacity for DOX and low biotoxicity. Further, the DOX-loaded MOGs show slow and sustainable releasing ability and high anticancer efficiency. MIL-100(Al) gels exhibit high qualities of all the performance-indicators as mentioned above, making DOX-loaded MOGs a promising anticancer approach for clinical application.

Supplementary Materials: The following are available online at www.mdpi.com/xxx/s1.

Author Contributions: Y.F. conceived and designed the experiments; Y.F. and C.W. performed the experiments; Y.F. and C.W. analyzed the data; Y.F. wrote the paper.

Acknowledgments: This work is supported by the National Key R&D Program of China (2017YFA0403402), the Natural Science Foundation of China (Grants U1732272 and 21773222), the Key Pro-gram of Research and Development of Hefei Science Center of CAS (2017HSC-KPRD001) and Collaborative Innovation Center of Suzhou Nano Science and Technology. Thanks for Mr. Jilong Wang and Dr. Fan Zheng for the assistance of in vivo cell experiments.

Conflicts of Interest: The authors declare no conflict of interest.

References

1. Jain, R.K.; Stylianopoulos, T. Delivering nanomedicine to solid tumors, *Nat. Rev. Clin. Oncol.* 2010, **7**, 653-664.
2. Davis, M.E.; Chen, Z.; Shin, D.M. Nanoparticle therapeutics: an emerging treatment modality for cancer, *Nat. Rev. Drug Discov.* 2008, **7**, 771-781.

3. Maeda, H.; Nakamura, H.; Fang, J. The EPR effect for macromolecular drug delivery to solid tumors: improvement of tumor uptake, lowering of systemic toxicity, and distinct tumor imaging in vivo, *Adv. Drug Deliv. Rev.* 2013, **65**, 71-79.
4. Chen, Y.; Ai, K.; Liu, J.; Sun, G.Y.; Yin, Q.; Lu, L.H.; Multifunctional envelope-type mesoporous silica nanoparticles for pH-responsive drug delivery and magnetic resonance imaging, *Biomaterials* 2015, **60**, 111-120.
5. Chowdhuri, A.R.; Singh, T.; Ghosh, S.K.; Sahu, S.K. Carbon dots embedded magnetic nanoparticles@chitosan@metal organic framework as a nanoprobe for pH sensitive targeted anticancer drug delivery. *ACS Appl. Mater. Interfaces* 2016, **8**, 16573-16583.
6. Su, Y.Y.; Teng, Z.; Yao, H.; Wang, S.J.; Tian, Y.; Zhang, Y.L.; Liu, W.F.; Tian, W.; Zheng, L. J.; Lu, N.; Ni, Q.Q.; Su, X.D.; Tang, Y.X.; Sun, J.; Liu, Y.; Wu, J.; Yang, G.F.; Lu, G. M.; Zhang, L.J. A multifunctional PB@mSiO2−PEG/DOX nanoplatform for combined photothermal−chemotherapy of tumor. *ACS Appl. Mater. Interfaces* 2016, **8**, 17038-17046.
7. Jalvandi, J.; White, M.; Gao, Y.; Truong, Y.B.; Padhye, R.; Kyratzis, I.L. Polyvinyl alcohol composite nanofibres containing conjugated levofloxacin-chitosan for controlled drug release, *Mater. Sci. Eng. C* 2017, **73**, 440-446.
8. Wang, D.D.; Zhou, J.J.; Chen, R.H.; Shi, R.H.; Zhao, G.Z.; Xia, G.L.; Li, R.; Liu, Z.B.; Tian, J.; Wang, H.J.; Guo, Z.; Wang, H.B.; Chen, Q.W. Controllable synthesis of dual-MOFs nanostructures for pH-responsive artemisinin delivery, magnetic resonance and optical dual-model imaging-guided chemo/photothermal combinational cancer therapy. *Biomaterials* 2016, **100**, 27-40.
9. Zhao, D.; Timmons, D.J.; Yuan, D.; Zhou, H.C. Tuning the Topology and Functionality of Metal−Organic Frameworks by Ligand Design, *Acc. Chem. Res.* 2011, **44**, 123-133.
10. Corma, A.; Garcia, H.; Llabres, F.X.; Xamena, I. Engineering Metal Organic Frameworks for Heterogeneous, *CatalysisChem. Rev.* 2010, **110**, 4606-4655.
11. Keskin, S.; Kizilel, S. Biomedical Applications of Metal Organic Frameworks, *Chem. Res.* 2011, **50**, 1799-1812.
12. Yang, X.L.; Chen, X.H.; Hou, G.H.; Guan, R.F.; Shao, R.; Xie, M.H. A multiresponsive metal–organic framework: direct chemiluminescence, photoluminescence, and dual tunable sensing applications, *Adv. Funct. Mater.* 2016, **26**, 393-398.
13. Kaur, R.; Kim, K.H.; Paul, A.K.; Deep, A. Recent advances in the photovoltaic applications of coordination polymers and metal organic frameworks, *J. Mater. Chem. A* 2016, **4**, 3991-4002.
14. Li, H.; Guo, K.; Wu, C.; Shu, L.; Guo, S.; Hou, J.; Zhao, N.; Wei, L.; Man, X.; Zhang, L. Controlled and Targeted Drug Delivery by a UV-responsive Liposome for Overcoming Chemo-resistance in Non−Hodgkin Lymphoma, *Chem. Biol. Drug Des.* 2015, **86**, 783-794.
15. He, Q.; Gao, Y.; Zhang, L.; Zhang, Z.; Gao, F.; Ji, X.; Li, Y.; Shi, J. A pH-responsive mesoporous silica nanoparticles-based multi-drug delivery system for overcoming multi-drug resistance, *Biomaterials* 2011, **32**, 7711-7720.
16. Nunzio, M.R.; Agostoni, V.; Cohen, B.; Gref, R.; Douhal, A. A "Ship in a Bottle" Strategy To Load a Hydrophilic Anticancer Drug in Porous Metal Organic Framework Nanoparticles: Efficient Encapsulation, Matrix Stabilization and Photodelivery, *J. Med. Chem.* 2014, **57**, 411-420.
17. Sun, K. K.; Li, L.; Yu, X. L.; Liu, L.; Meng, Q. T.; Wang, F.; Zhang, R. Functionalization of mixed ligand metal-organic frame-works as the transport vehicles for drugs, *J. Colloid Interface Sci.* 2017, **486**, 128-135.
18. Vasconcelos, I.B.; Silva, T.G.; Militao, G.C.; Soares, T.A.; Rodrigues, N.M.; Rodrigues, M.O.; Freire, N.B.; Junior, S.A. Cytotoxicity and slow release of the anti-cancer drug doxorubicin from ZIF-8, *RSC Adv.* 2012, **2**, 9437-9442.
19. Sengupta, S.; Mondal, R. Metal-Organic-Particle-Supported Metallogel Formation Using a Nonconventional Chelating Pyridine-Pyrazole-Based Bis-Amide Ligand, *Chem. Eur. J.* 2013, **19**, 5537-5541.
20. Zhang, J.; Su, C.Y. Metal-organic gels: From discrete metal-logelators to coordination polymers, *Coordin. Chem. Rev.* 2013, **257**, 1373-1408.
21. Xiao, B.; Zhang, Q.; Huang, C.; Li, Y. Luminescent Zn(ii)–terpyridine metal organic gel for visual recognition of anions, *RSC Adv.* 2015, **5**, 2857-2860.
22. Aiyappa, H. B.; Saha, S.; Wadge, P.; Banerjee, R. S. Fe(III) phytate metallogel as a prototype anhydrous, intermediate temperature proton conductor, *Chem. Sci.* 2015, **6**, 603-607.

23. Huang, M.; Mi, K.; Zhang, J.H.; Liu, H.L.; Yu, T.T.; Yuan, A.; Kong, Q.; Xiong, S. MOF-derived bi-metal embedded N-doped carbon polyhedral nanocages with enhanced lithium storage, *J. Mater. Chem. A* 2017, **5**, 266-274.
24. Zhao, X.; Yuan, L.; Zhang, Z. Q.; Wang, Y. S.; Yu, Q.; Li, J. Synthetic Methodology for the Fabrication of Porous Porphyrin Materials with Metal-Organic-Polymer Aerogels, *Inorg. Chem*. 2016, **55**, 5287-5296.
25. Li, L.; Xiang, S. L.; Cao, S. Q.; Zhang, J. Y.; Ouyang, G. F.; Chen, L. P.; Su, C. Y. A synthetic route to ultralight hierarchically micro/mesoporous Al(III)-carboxylate metal-organic aerogels, *Nat. Commun.* 2013, **4**, 1774-1782.
26. Mahmood, A.; Xia, W.; Mahmood, N.; Wang, Q. F.; Zou, R. Q. Hierarchical heteroaggregation of binary metal-organic gels with tunable porosity and mixed valence metal sites for removal of dyes in water, *Sci. Rep.* 2015, **5**, 10556-10568.
27. Sutar, P.; Maji, T. K. Coordination polymer gels: soft metal–organic supramolecular materials and versatile applications, *Chem. Commun.* 2016, **52**, 8055-8074.
28. Liu, Y.R.; He, L.; Zhang, J.; Wang, X.; Su, C.Y. Evolution of spherical assemblies to fibrous networked Pd (II) metallo gels from a pyridine-based tripodal ligand and their catalytic property, *Chem. Mater.* 2009, **21**, 557-563.
29. Tan, S.Y.; Ang, C.Y.; Mahmood, A.; Qu, Q.; Li, P.; Zou, R. Zhao, Y.L. Doxorubicin-Loaded Metal-Organic Gels for pH and Glutathione Dual-Responsive Release. *ChemNanoMat* 2016, **2**, 504-508.
30. Kayal, S.; Ramanujan, R.V. Doxorubicin loaded PVA coated iron oxide nanoparticles for targeted drug delivery, *Mater. Sci. Eng. C* 2010, **30**, 484-490.